Neurobiology of Aging 120 (2022) 68–80

Contents lists available at ScienceDirect

Neurobiology of Aging

journal homepage: www.elsevier.com/locate/neuaging.org

White matter degradation near cerebral microbleeds is associated with cognitive change after mild traumatic brain injury

Andrei Irimia[a,b,*], Van Ngo[a], Nikhil N. Chaudhari[a], Fan Zhang[c], Shantanu H. Joshi[d], Anita N. Penkova[e], Lauren J. O'Donnell[c], Nasim Sheikh-Bahaei[f,g], Xiaoyu Zheng[h], Helena C. Chui[g]

[a] Ethel Percy Andrus Gerontology Center, Leonard Davis School of Gerontology, University of Southern California, Los Angeles, CA, USA
[b] Denney Research Center, Department of Biomedical Engineering, Viterbi School of Engineering, University of Southern California, Los Angeles, CA, USA
[c] Laboratory of Mathematics in Imaging, Department of Radiology, Brigham & Women's Hospital, Harvard Medical School, Boston, MA, USA
[d] Ahmanson Lovelace Brain Mapping Center, Department of Neurology, David Geffen School of Medicine, University of California, Los Angeles, CA, USA
[e] Department of Aerospace and Mechanical Engineering, Viterbi School of Engineering, University of Southern California, Los Angeles, CA, USA
[f] Department of Neurology, Keck School of Medicine, University of Southern California, Los Angeles, CA, USA
[g] Department of Radiology, Keck School of Medicine, University of Southern California, Los Angeles, CA, USA
[h] Department of Materials Science & Engineering, University of California, Berkeley, CA, USA

ARTICLE INFO

Article history:
Received 17 November 2021
Revised 17 August 2022
Accepted 20 August 2022
Available online 24 August 2022

Keywords:
Neurovascular injury
Brain atrophy
Brain aging
Connectome atrophy
Cognitive decline

ABSTRACT

To explore how cerebral microbleeds (CMBs) accompanying mild traumatic brain injury (mTBI) reflect white matter (WM) degradation and cognitive decline, magnetic resonance images were acquired from 62 mTBI adults (imaged ~7 days and ~6 months post-injury) and 203 matched healthy controls. On average, mTBI participants had a count of 2.7 ± 2.6 traumatic CMBs in WM, located 6.1 ± 4.4 mm from cortex. At ~6-month follow-up, 97% of CMBs were associated with significant reductions (34% ± 11%, $q < 0.05$) in the fractional anisotropy of WM streamlines within ~1 cm of CMB locations. Male sex and older age were significant risk factors for larger reductions ($q < 0.05$). For CMBs in the corpus callosum, cingulum bundle, inferior and middle longitudinal fasciculi, fractional anisotropy changes were significantly and positively associated with changes in cognitive functions mediated by these structures ($q < 0.05$). Our findings distinguish traumatic from non-traumatic CMBs by virtue of surrounding WM alterations and challenge the assumption that traumatic CMBs are neurocognitively silent. Thus, mTBI with CMB findings can be described as a clinical endophenotype warranting longitudinal cognitive assessment.

© 2022 Elsevier Inc. All rights reserved.

1. Introduction

Over 1.7 million Americans suffer traumatic brain injuries (TBIs) every year, resulting in an all-time TBI prevalence greater than ~15% in US adults (Wu et al., 2016). In mild TBI (mTBI), acute clinical brain scans acquired using T_1- and T_2-weighted magnetic resonance imaging (MRI) are frequently free of radiological findings even in cases where neurocognitive deficits persist for many months post-injury (Shenton et al., 2012). By contrast, even in the absence of T_1-weighted or T_2-weighted MRI findings, susceptibility weighted images (SWIs) exhibit cerebral microbleeds (CMBs) commonly in mTBI patients (Park et al., 2009; Tate et al., 2017; Toth et al., 2013), and CMB counts are associated with both TBI severity (van der Eerden et al., 2021) and patient age at injury (Robles et al., 2022; Toth et al., 2021). CMBs reflect the ferromagnetic effects of iron-containing hemosiderin left from microhemorrhage and breakdown in the blood brain barrier (BBB). CMBs are commonly associated with small vessel disease, for example, involving hypertensive hyaline necrosis in deep penetrating arterioles and cerebral amyloid angiopathy (CAA) in cortical arterioles (Martinez-Ramirez et al., 2014); hypertensive or amyloid related CMBs may also antedate mTBI (Mosenthal et al., 2004). In the setting of mTBI, on the other hand, CMBs result from mechanical stress on cerebral microvessels and surrounding tissues, and are typically located near interfaces between white matter (WM) and gray matter (GM) (Bigler and Maxwell, 2012; Glushakova et al., 2014; Lok et al., 2011; Petrault et al., 2019). The relationships between mTBI-related CMBs, WM integrity/connectivity and cognitive deficits has not been quantified *in vivo*.

* Corresponding author at: Ethel Percy Andrus Gerontology Center, Leonard Davis School of Gerontology, University of Southern California, 3715 McClintock Avenue, Suite 228, Los Angeles CA 90089 USA.
E-mail address: irimia@usc.edu (A. Irimia).

0197-4580/$ – see front matter © 2022 Elsevier Inc. All rights reserved.
https://doi.org/10.1016/j.neurobiolaging.2022.08.010

Diffusion MRI (dMRI) is frequently used to map WM bundle trajectories *in vivo*. Measures like the fractional anisotropy (FA) of water diffusion within WM can identify brain locations whose WM properties change significantly after TBI relative to healthy controls (HCs) (Eierud et al., 2014). Although mTBI effects on WM have been investigated (Hellyer et al., 2013), the spatial and temporal relationships between CMBs and surrounding WM changes is largely unknown due to the challenge of evaluating such changes. Nevertheless, establishing the associations of post-traumatic CMBs with WM degradation and cognitive decline is important because CMBs are identified ubiquitously on neuroradiological mTBI examinations. If post-traumatic CMBs are significantly associated with cognitive decline, CMB findings could assist the difficult task of stratifying mTBI patients according to their cognitive prognosis. Stratification based on post-traumatic CMB findings could benefit especially older patients, who may have greater BBB permeability and more inadequate neuroinflammatory responses (Irimia et al., 2015; Irimia et al., 2018; Wu et al., 2016). However, older adults also have a higher likelihood of exhibiting pre-/non-traumatic CMBs (Jeerakathil et al., 2004). Thus, effective strategies for stratifying older mTBI patients based on CMB findings could benefit from the ability to resolve CMB etiology, which is potentially ambiguous.

Our previous study (Rostowsky et al., 2018) provided initial evidence that CMBs identified on post-traumatic MRIs are associated with persisting WM alterations. In this study, we introduce an analytic framework to evaluate WM changes related to mTBI-related CMBs. Our approach leverages a detailed dMRI atlas to label WM fasciculi and to categorize them into WM bundle clusters (O'Donnell et al., 2009; Zhang et al., 2018). When utilized in conjunction with longitudinal WM streamline matching (O'Donnell et al., 2009; Rostowsky et al., 2018), this approach facilitates our fiducial identification of WM bundles across timepoints and the quantification of WM changes near CMBs. We synergize these strategies with a novel probabilistic inference framework to quantify the likelihood that a CMB is of traumatic etiology. To our knowledge, these analytic solutions are the first of their kind in the field of neuroimage analysis. We use our novel approaches to test the hypothesis that WM integrity loss (i.e., FA decrease) near CMBs can differentiate traumatic from vascular ones. For CMBs that are significantly likely to be of traumatic etiology, we test the null hypothesis that, across the first ∼6 months post-injury, there is no WM diffusion property change near the CMBs. Finally, the hypothesis of no association between these changes and participants' cognitive changes is tested to assess whether CMBs modulate cognitive decline.

2. Methods

2.1. Participants

Participants provided written informed consent as required by the Declaration of Helsinki, US 45 CFR 46, and neuroimage volume acquisition was conducted with the approval of ethics committees at the respective institutions where data were acquired. Datasets were anonymized and adequate measures were taken in compliance with the US Health Insurance Portability and Accountability Act (HIPAA) to ensure that participants' confidentiality and identities would be preserved. Cohort demographics are summarized in Table 1. Participants with mTBI ($N = 62$, 36 males; age: mean $\mu = 44$ years (y), standard deviation $\sigma = 18$ y, range: 19–79 y) were recruited as outpatients in a hospital setting. Inclusion criteria were (1) a single mTBI due to a fall, (2) MRIs acquired at 3 T both shortly after injury (7.4 ± 3.2 days) and approximately 6 months later (5.8 ± 0.4 months), (3) no radiological findings on acute T_1/T_2-weighted MRI other than WM hyperintensities potentially unrelated to mTBI, (*4*) no SWI findings other than CMBs, (*5*) acute Glasgow Coma Scale (GCS) scores greater than 12 upon initial clinical evaluation, (*6*) post-traumatic loss of consciousness (LOC) of less than 30 minutes, (*7*) post-traumatic amnesia (PTA) of less than 24 hours, and (*8*) no pre-traumatic clinical history of neurological disease, psychiatric disorder or drug/alcohol abuse. mTBI participants' Montréal Cognitive Assessment (MoCA) scores (Nasreddine et al., 2005) were obtained within 48 hours post-injury and ∼6 months post-injury. Typically, MoCA was administered several days before MRI acquisition due to scanner scheduling constraints. HCs were scanned twice within time intervals comparable to those of mTBI follow-ups and had neither MRI findings nor histories of drug/alcohol abuse, neurological or psychiatric disease. Two HC groups were included: (1) HCs *without* CMB findings (CMB^-) on SWI ($N = 153$; 83 males; age $\mu = 55$ y, $\sigma = 15$ y, range: 21–87 y), and (2) HCs *with* CMB findings (CMB^+) on SWI ($N = 50$; 25 males; age $\mu = 74$ y, $\sigma = 8$ y, range: 56–91 y). HCs were recruited from the community and had no known history of TBI.

2.2. Neuroimaging

MRIs were obtained from mTBI and HC participants using similar protocols (Fig. 1A). T_1-weighted MRIs were acquired at 3 T (Trio TIM scanner, Siemens Corp., Erlangen, Germany) using a 3-dimensional, magnetization-prepared rapid acquisition gradient echo sequence [repetition time (T_R) = 1950 ms; echo time (T_E) = 2.98 ms; inversion time (T_I) = 900 ms; voxel size = 1.0 mm × 1.0 mm × 1.0 mm]. T_2-weighted images were acquired using a 3D sequence ($T_R = 2500$ ms; $T_E = 360$ ms; voxel size = 1.0 mm × 1.0 mm × 1.0 mm). Flow-compensated GRE/SWI volumes were acquired axially ($T_R = 30$ ms; $T_E = 20$ ms; voxel size = 1.33 mm × 1.33 mm × 1.6 mm; acquisition matrix size = 256 × 256; phase field of view (FOV) = 100%; number of slices = 128; number of echoes = 1). Fluid-attenuated inversion recovery (FLAIR) volumes were acquired using a 3D syngo sequence ($T_R = 6000$ ms; $T_E = 390$ ms; $T_I = 2100$ ms; voxel size = 0.5 mm × 0.5 mm × 1.2 mm; acquisition matrix size = 256 × 242; phase FOV = 93.75%; number of slices = 176). dMRI volumes were acquired axially in 64 gradient directions using a readout segmentation of long variable echo-trains (RESOLVE) Syngo sequence ($T_R = 8300$ ms; $T_E = 72$ ms; voxel size = 2.7 mm × 2.7 mm × 2 mm). One volume with $b = 0$ s/mm^2 and another with $b = 1000$ s/mm^2 were also acquired (the latter in 64 gradient directions), where b is the constant of diffusion weighted imaging. For purposes pertaining to this study, all data were analyzed retrospectively.

2.3. Preprocessing

FreeSurfer (FS) software with default parameters was used to strip the skull, segment the brain, and reconstruct both pial and WM surfaces from T_1-weighted MRIs (Fig. 1B). SWIs were co-registered rigidly to T_1-weighted MRIs and then skull-stripped using the FS brain mask (Fig. 1C). For dMRI, using a pair of images with opposite phase encoding directions, artifacts induced by susceptibility were estimated (Andersson et al., 2003) and FSL software was used to implement motion and eddy current artefact corrections (Fig. 1D). The B vectors of each volume were rotated to account for inadequate rotations due to patient motion. DWI volumes were processed in FSL by fitting tensors to corrected DWI volumes to undertake diffusion tensor imaging (DTI), including DT estimation and 2-tensor tractography, in 3DSlicer (Fig. 1D). Tractography was performed using unscented Kalman filter (UKF) 2-tensor tractography with seeds across the whole brain and using 1

Table 1
Cohort demographics and descriptors

Demographic		mTBI				CMB$^-$ HCs				CMB$^+$ HCs			
sample size		62				153				50			
males:females		36:26				83:70				25:25			
descriptor	units	μ	σ	min	max	μ	σ	min	max	μ	σ	min	max
age	years	44.0	18.0	19.0	79.0	55.0	15.0	21.0	87.0	74.0	8.0	56.0	91.0
acute MRI	days	7.0	3.0	2.0	14.0	0.0	0.0	0.0	0.0	0.0	0.0	0.0	0.0
chronic MRI	months	5.8	0.4	5.1	6.8	6.1	0.7	5.4	7.5	6.3	0.9	5.1	8.3
CMB	count	7.8	4.9	1.0	14.0	0.0	0.0	0.0	0.0	1.6	1.0	1.0	6.0
LOC	minutes	14.0	3.0	0.0	22.0								
PTA	hours	5.5	3.2	0.2	8.6								
acute MoCA		27.0	4.0	22.0	30.0								
chronic MoCA		28.0	5.2	20.0	30.0								
GCS		14.1	0.7	13.0	15.0								

For HCs, data are reported separately for CMB-negative (CMB$^-$) and CMB-positive (CMB$^+$) participants.

seed per voxel and default parameters (Liao et al., 2017). For example, seed points with FA below 0.18 were excluded. Tractography stopped when (1) the FA of the tensor being tracked was less than 0.15 or (2) the mean signal was below 0.1. The tractography step length was set to 0.3 mm. The step size between points saved along streamlines was set to 0.9 mm. If a streamline exhibited a turning angle below 60 degrees, it was discarded. WM bundles shorter than 4 cm were discarded because the WM clustering algorithm used is unsuitable for identifying streamlines shorter than this. DTI volumes were used for voxel-wise calculations of 4 *diffusion metrics*, namely FA, axial diffusivity (AD), radial diffusivity (RD), and mean diffusivity (MD).

2.4. WM clustering

A neuroanatomist-curated streamline clustering atlas (Zhang et al., 2018) was used for WM streamline labeling (Fig. 1E). This atlas classifies cerebral WM connections into ~800 WM clusters using an annotation approach integrating population-based neuroanatomical information and expert neuroanatomical knowledge. The annotation is incorporated within an atlas containing deep WM clusters (including prominent long-range projection and association bundles), cerebellar connections, and commissural bundles. The atlas includes superficial medium- and short-range clusters categorized based on their inter-lobar connectivity.

2.5. Streamline prototyping

Streamline prototyping was used to identify clusters' representative streamlines (O'Donnell and Westin, 2007; O'Donnell et al., 2009; Rostowsky et al., 2018) (Fig. 1E). This involves analyzing each cluster to find a single streamline within it whose geometric properties are representative of the cluster's streamline trajectories and properties. Prototyping is necessary in studies like ours because tractography may yield artefactual streamlines that do not correspond to physical connectivity. By contrast, a cluster's prototype streamline is fiducially representative of the cluster's architecture, structure, and properties (O'Donnell et al., 2009). Weighted means of diffusion metrics (FA, AD, RD, MD) were calculated along each cluster's prototype streamline, that is, across all voxels spanned by the cluster. This weighted mean reflects the extent to which every cluster streamline's properties contribute to those of the streamline prototype at each location along it.

2.6. Streamline matching

To account for within-participant variance in prototype streamline properties across imaging sessions, points along each prototype streamline were matched across sessions (Fig. 1E). Streamlines were modeled as shapes using square root velocity functions (Joshi et al., 2007; Prasad et al., 2014; Srivastava et al., 2011) within an algorithm involving Riemannian curve matching, where geodesics (shortest-length paths) are calculated between curves matched across time points. Geodesics provide path lengths, quantify geometric distances between streamlines, and define optimal geometric deformations that highlight anatomical differences between them. Streamlines' maximum density paths and geodesics were calculated within participants and across time points.

2.7. CMB identification

CMBs were identified by 8 human raters with training in neuroimaging and in CMB delineation from magnitude SWIs (Sehgal et al., 2005). Consensus meetings to review CMB findings were held by 3 of the 8 raters (Fig. 1F); each finding was reviewed thoroughly until consensus was reached on its accuracy. Then, the shortest distance between each CMB and the cortex was calculated. For any CMB, *proximal* WM was defined to include WM streamline portions located within topological distances of ~10 mm from the CMB. Similarly, *distal* WM was defined as the set of streamline segments located between ~10 and ~20 mm from the CMB.

2.8. CMB specificity for mTBI etiology

By comparing each mTBI participant to all other mTBI participants as well as to 2 age- and sex-matched HC groups, this study relied on a multi-step procedure to estimate the probability that each CMB was of traumatic etiology (Fig. 2). This procedure was implemented for each CMB of every participant while accounting for age and sex effects. The groups to whom each mTBI participant was compared included: (1) HCs without CMB, (2) all participants with mTBI excluding the participant being compared, and (3) HCs with pre-existing CMBs. Because (1) FLAIR hyperintensities surrounding CMBs are typically indicative of acute edema onset soon after CMB occurrence and (2) the patients had no history of TBI prior to the mTBI for which they were imaged in this study, the absence of FLAIR hyperintensities around the CMBs of CMB$^+$ HCs indicates that the neurovascular events prompting CMB occurrence in HCs were unlikely to be recent.

In step 1, we tested a null hypothesis to discount the possibility that phenomena unrelated to mTBI (e.g., natural aging) accounted for the observed association between CMBs and changes in their proximal WM. Specifically, we tested the null hypothesis that (1) the change in the mean of each diffusion metric (FA, AD, RD, MD) near a CMB was equal to (2) the mean change in the respective metric, measured across HCs without CMBs, near a *simulated* CMB

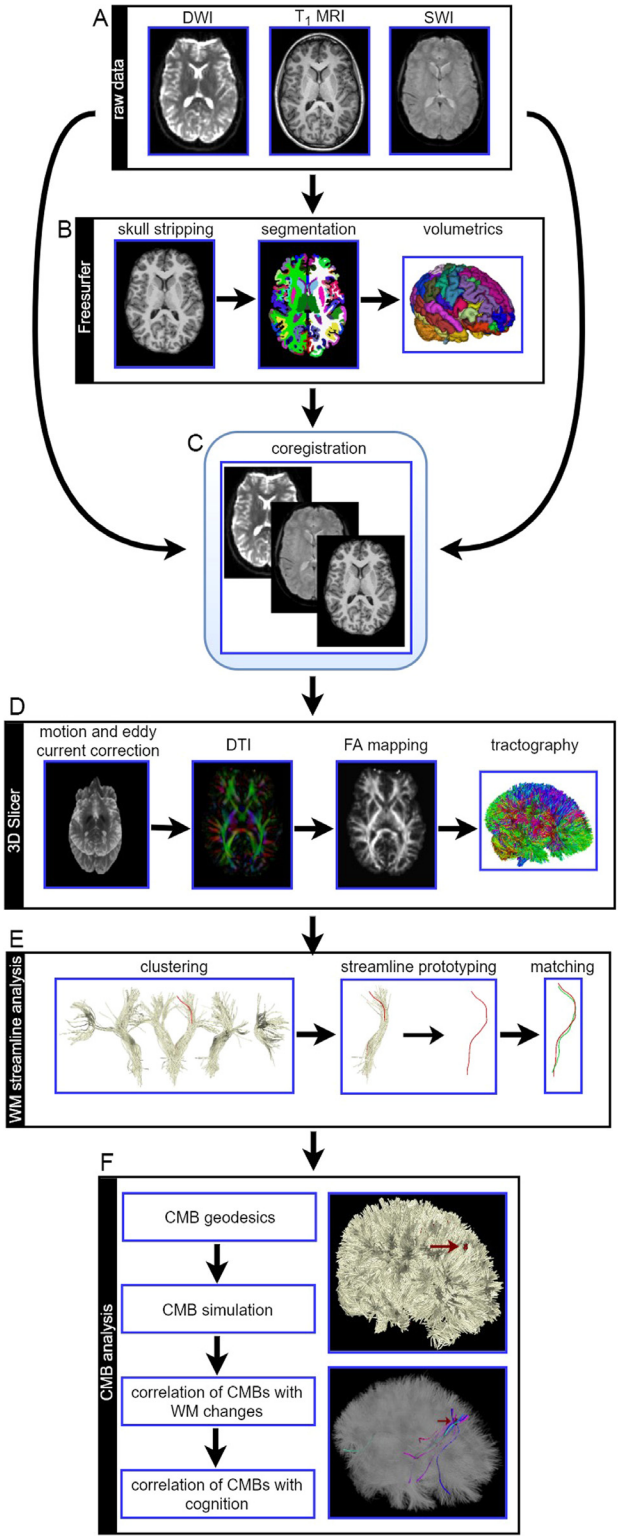

Fig. 1. Neuroimage and quantitative analysis workflow. (A) MRIs are obtained from mTBI and HC participants. (B) FS software is used to strip the skull, segment the brain, and reconstruct pial and white matter (WM) surfaces. (C) MRIs are co-registered across modalities and time points. (D) After correcting motion and eddy current artefacts, DTI helps to map FA and obtain tractography. (E) A neuroanatomist-curated streamline clustering atlas is used for WM streamline labeling, followed by streamline prototyping and matching across time points. (F) After CMB identification (for mTBI participants) or simulation (for HC participants), CMB geodesics are calculated, CMB correlations with WM changes are computed, and study hypotheses are tested. (For interpretation of the references to color in this figure legend, the reader is referred to the Web version of this article.)

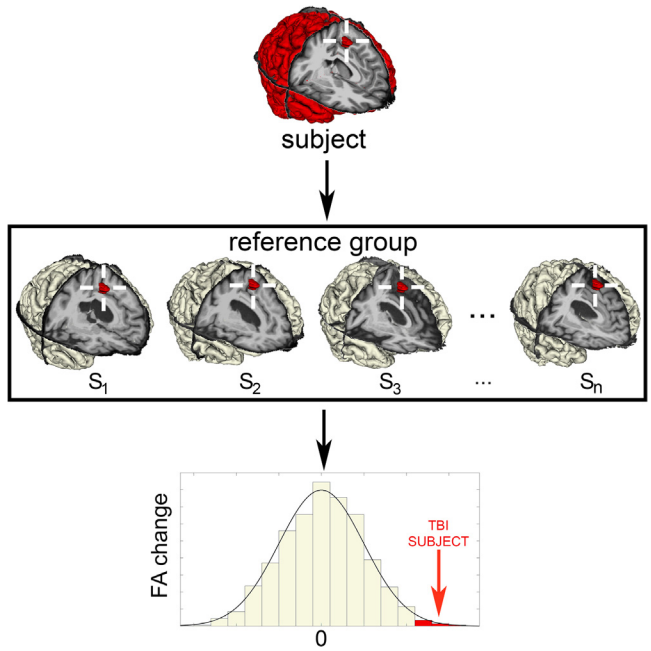

Fig. 2. Tripartite hypothesis testing framework. By comparing each mTBI participant (red-colored brain, top) to a reference group of size n containing participants S_1, S_2, …, S_n (white-colored brains, center), the probability that each CMB (within crosshairs) had a traumatic etiology was calculated based on a 3-step procedure (see section 2.8) using hypothesis tests involving the distribution of FA values proximal to the CMB (bottom). The reference group is different in each of the 3 steps of the hypothesis testing procedure (see section 2.8). (For interpretation of the references to color in this figure legend, the reader is referred to the Web version of this article.)

at the same standardized brain coordinates as the mTBI participant's *genuine* CMB. Rejection of this null hypothesis was interpreted as indication that the mTBI participant's mean change in a diffusion metric near the CMB was likely related to mTBI rather than to non-traumatic biological processes such as natural aging. The hypothesis was also tested separately at each time point by comparing (1) the mean of the diffusion metric (rather than mean *change* in the diffusion metric) near a genuine CMB to (2) the mean value of the diffusion metric (rather than to the mean *change* in the diffusion metric) near a simulated CMB.

In step 2, we tested a null hypothesis to discount the possibility that mTBI-related phenomena unrelated to CMBs accounted for the observed association between CMBs and changes in their proximal WM. Specifically, we tested the null hypothesis that (1) the mean change in a diffusion metric near the mTBI participant's CMB was equal to (2) the mean, computed across all other mTBI participants, of the change in the respective diffusion metric near a *simulated* CMB at the same standardized brain coordinates as the mTBI participant's *genuine* CMB. Rejection of this null hypothesis was interpreted as indication that the mTBI participant's change in the diffusion metric near the CMB was likely related to this specific CMB rather than to trauma-induced changes common to all mTBI participants. The hypothesis was also tested separately at each time point by comparing (1) the mean *value* of the diffusion metric (rather than mean *change* in the diffusion metric) near the TBI participant's CMB to (2) the mean *value* of the respective diffusion metric (rather than to the mean *change* in the diffusion metric) near a simulated CMB at the same standardized coordinates as the genuine CMB.

In step 3, we tested a null hypothesis to discount the possibility that *non-traumatic* phenomena related to CMBs accounted for the observed association between CMBs and changes in their prox-

imal WM. Specifically, we tested the null hypothesis that (1) the mean change in a diffusion metric near the mTBI participant's CMB was equal to (2) the mean, computed across CMB^+ HCs, of the change in the diffusion metric near a *genuine* CMB at similar standardized brain coordinates as the mTBI participant's CMB. Rejection of this null hypothesis was interpreted as indication that the change in the mean of the diffusion metric near the mTBI participant's CMB proceeded at a rate different from that observed near non-traumatic CMBs. The hypothesis was also tested separately at each time point by comparing (1) the mean of the diffusion metric (rather than the mean *change* in the diffusion metric) near the CMB to (2) the mean of the diffusion metric (rather than to the mean *change* in the diffusion metric), across CMB^+ HCs, near a genuine CMB at the same standardized coordinates as the genuine CMB.

All hypotheses were tested at $\alpha = 0.05$, subject to multiple comparison correction. Failure to reject all 3 null hypotheses pertaining to *changes* in diffusion metric was interpreted as indication that the mTBI participant's CMB was likely unrelated to biological processes that were (1) distinct from those prompted by mTBI, (2) prompted by mTBI but distinct from processes associated with CMBs, or (3) associated with non-traumatic CMBs. Thus, failure to reject all 3 null hypotheses involving changes in diffusion metric was interpreted as indicating that an mTBI participant's CMB was of likely traumatic etiology. All 3 hypotheses were tested while accounting for individual deviations from the group average of the follow-up interval.

2.9. Spatially proximal versus distal WM changes

For every CMB in each mTBI participant, we compared (1) diffusion metric changes that were spatially closest (proximal) to the CMB, on the one hand, to (2) diffusion metric changes farther (distal) from the CMB, on the other hand. All diffusion metric changes in question were measured across the follow-up interval. The null hypothesis that (1) the mean diffusion metric change near an mTBI participant's CMB is equal to (2) the mean diffusion metric change distal to the CMB was tested at $\alpha = 0.05$, with Benjamini-Hochberg corrections to control the false discovery rate (FDR, $q < 0.5$). Effects pertaining to interscan interval, age, sex and to their interaction were accounted for within a general linear model (GLM) that included acute GCS score and LOC duration as covariates. The null hypothesis was also tested separately at each time point to compare (1) the mean diffusion metric (rather than the mean diffusion metric *change*) near an mTBI participant's CMB to (2) the mean diffusion metric (rather than to the mean diffusion metric *change*) distal to the CMB.

2.10. CMB distance versus WM changes

After identifying CMBs of likely traumatic etiology (section 2.8), we quantified the statistical relationship between (1) diffusion metric changes along the prototype streamlines of WM structures proximal to each CMB, and (2) the topological distances from the CMB to points on these streamlines. For each CMB in every mTBI participant, we tested the null hypothesis that, as the topological distance between the CMB and each point on the prototype streamline increases, the correlation between this distance and the diffusion metric change measured along the streamline is equal to zero (Fig. 3A). Biologically, this hypothesis is important because its confirmation indicates that mTBI-related CMBs have no significant longitudinal effects upon nearby WM connectivity. The alternative hypothesis suggests that a CMB is associated with diffusion metric changes whose magnitudes decrease as the distance to the CMB increases (Fig. 3B). In other words, according to the alternative hypothesis, the farther a point is from a CMB, the lower the value of the diffusion metric is at that point. Biologically, the alternative hypothesis is important because it allows us to identify mTBI-related CMBs that have a statistically significant effect upon nearby WM connections. The null hypothesis was also tested separately for each time point by examining the correlation between the CMB-to-streamline distance and each diffusion metric (rather than the diffusion metric *change*) along the streamline.

2.11. Cognitive change versus proximal changes along WM streamlines

We quantified the statistical relationship between (1) diffusion metric changes proximal to CMBs and (2) changes in MoCA subscores for attention, executive function, memory, language, and visuo-construction (Nasreddine et al., 2005). For each CMB in every mTBI participant, we identified the cluster and corresponding fasciculus within which the CMB was located. Then, the mean diffusion metric change that was proximal (i.e., closest) to the CMB was calculated over the prototype streamlines within this fasciculus. The correlation coefficient r was calculated between (1) the change in a MoCA sub-score and (2) the mean diffusion metric change that was proximal (i.e., closest) to the CMB within the fasciculus containing the CMB. The null hypothesis of no significant r was tested at $\alpha = 0.05$, subject to multiple comparison correction for the FDR. For each MoCA sub-score and WM structure harboring CMBs, failure to accept the null hypothesis is equivalent to the statement that the mean diffusion metric change observed in fascicular regions closest to the CMB is significantly associated with the observed MoCA sub-score change. In other words, rejection of the null hypothesis suggests that diffusion metric changes are associated with cognitive changes. Effects of age, sex and their interaction were accounted for in a GLM that included acute GCS score and LOC duration as covariates. The null hypothesis was also tested separately at each timepoint by evaluating the significance of the correlation between each MoCA sub-score (rather than each MoCA sub-score *change*) and the mean diffusion metric (rather than mean diffusion metric *change*) near the CMB.

3. Results

3.1. Demographics and CMB findings

Demographics are summarized in Table 1. mTBI participants' baseline scans were acquired 7.4 ± 3.2 days post injury; follow-up scans were acquired 5.8 ± 0.4 months post injury. GCS scores ranged from 13 to 15 ($\mu = 14.1$, $\sigma = 0.7$). There were 13 participants with an acute GCS score of 13, 30 with a score of 14, and 19 with a score of 15. On average, LOC lasted for $\mu = 14$ minutes ($\sigma = 3$ minutes); PTA lasted for $\mu = 5.5$ hours ($\sigma = 3.2$ hours). At baseline, the average MoCA score was $\mu = 27$ ($\sigma = 4$, range: 22–30); at follow-up, it was $\mu = 28$ ($\sigma = 5$, range: 20–30). The ages of CMB^- HCs differed significantly from those of mTBI participants (Welch's $t_{203} = -4.3$, $p = 1.3 \times 10^{-5}$), as did those of CMB^+ HCs (Welch's $t_{194} = -15.6$, $p = 9.3 \times 10^{-25}$). Across 50 CMB^+ HCs, 79 CMBs were identified; no participant had FLAIR hyperintensities surrounding their CMBs at either time point. The average CMB count was 1.6 ± 1.0 (range: 1–6; median: 1). No significant CMB count difference distinguished HC males from HC females (Welch's $t_{46} = 0.14$, $p = 0.89$). On average, cortical CMBs were located 6.1 ± 4.4 mm from the GM/WM junction, in temporal (46%, distance: 16.4 ± 15.1 mm), frontal (29%, 12.4 ± 11.0 mm), parietal (10%, 13.4 ± 13.8 mm), insular

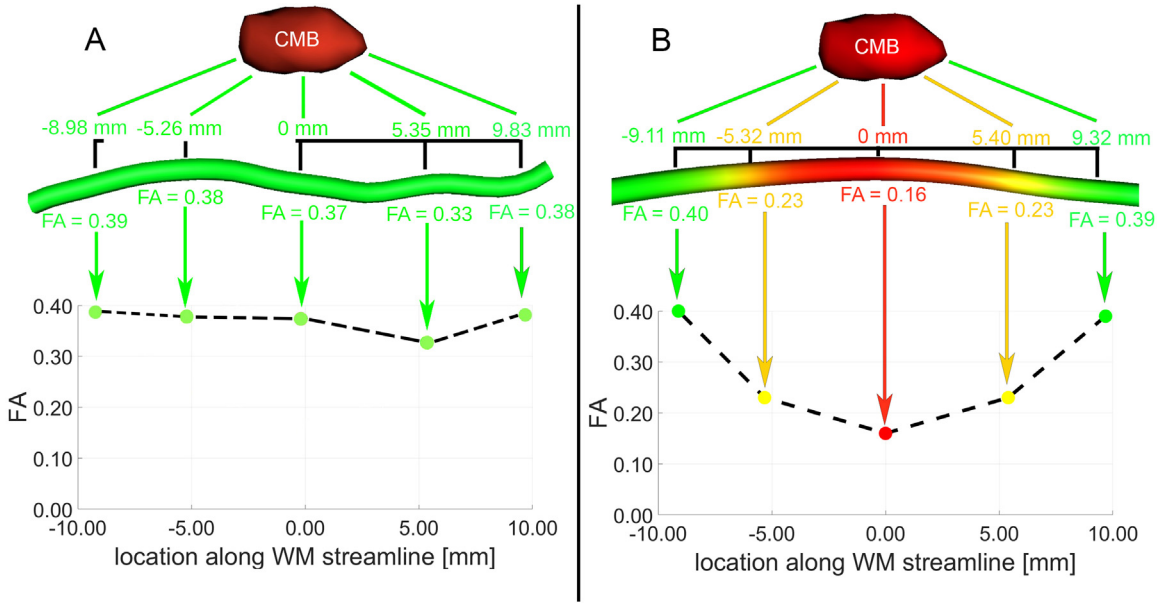

Fig. 3. WM changes near traumatic CMBs. Visualization of the statistical relationship between FA changes along the prototype streamline (colored tube) proximal to a CMB, on the one hand, and distances (in mm) from the CMB to points on the streamline, on the other hand. (A) Null hypothesis (non-traumatic CMB scenario). There is no significant relationship between FA changes along the prototype streamline, on the one hand, and the distance from the CMB to points on the streamline, on the other hand. (B) Alternative hypothesis (traumatic CMB scenario). As the distance from the CMB to each point on the prototype streamline increases, the FA along the streamline increases, suggesting that the presence of the CMB is associated with lower FA near the CMB. (For interpretation of the references to color in this figure legend, the reader is referred to the Web version of this article.)

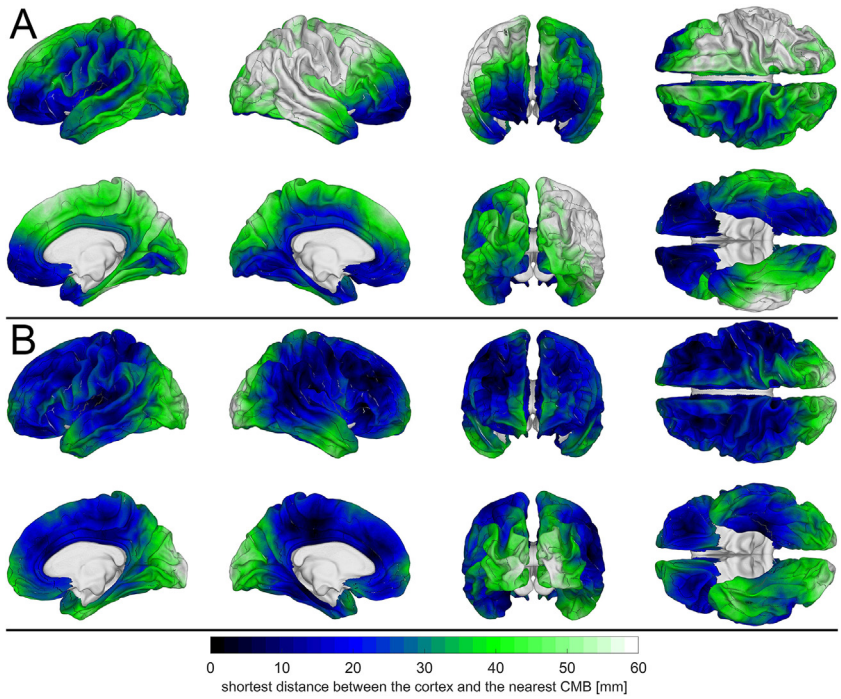

Fig. 4. Spatial distribution of traumatic CMBs. Mean shortest distance from the GM/WM interface to the nearest CMB for (A) CMB^{+} HCs and (B) mTBI participants are displayed. The distance between each vertex on the cortical mesh and the nearest CMB was computed for each participant, overlain on the cortical surface, and averaged across participants. CMBs are located near the cortex across the lateral and medial aspects of all lobes, with predominance in orbitofrontal and dorsolateral prefrontal cortices.

(10%, 5.9 ± 7.5 mm), or occipital (5%, 13.6 ± 13.9 mm) regions (Fig. 4A).

Across 62 mTBI participants, 173 CMBs were identified. The average CMB count was 2.7 ± 2.6 ($\mu \pm \sigma$; range: 1–14; median: 2). Whereas mTBI volunteers under 65 had 2.7 ± 2.5 CMBs (range: 1-14; median: 2), those over 65 had 3.4 ± 1.6 CMBs (range: 1–6; median: 3), a significant difference (t_{60} = -1.83, p = 0.04). No significant CMB count difference distinguished younger from older adults (Welch's t_{60} = -1.10, $p > 0.14$), or males from females (Welch's t_{60} = 0.43, p = 0.33). On average, cortical CMBs were located 6.1 ± 4.4 mm from the GM/WM junction, in frontal (50%, distance: 4.9 ± 3.2 mm), temporal (18%, 3.6 ± 2.9 mm), parietal (14%, 3.0 ± 3.0

mm), limbic (10%, 6.8 ± 8.8 mm), occipital (7%, 8.5 ± 5.5 mm) or insular (1%, 7.8 ± 3.7 mm) regions (Fig. 4B). CMB count was not significantly correlated with acute GCS score (r = -0.14, t_{60} = -1.10, p = 0.14), LOC duration (r = 0.13, t_{60} = 1.02, p = 0.16), PTA duration (r = 0.11, t_{60} = 0.86, p = 0.20), or MoCA score at follow-up (r = 0.14, t_{60} = 1.10, p = 0.14).

When using FA maps for our 3-step procedure to infer CMB etiology, all 62 mTBI participants were found to have at least one CMB of likely traumatic etiology ($q < 0.05$), and 166 (97%) CMBs were found likely to be traumatic. Thus, based on FA, each mTBI participant had at least one CMB of likely traumatic etiology according to this analysis, and only these 166 CMBs were included in subsequent analyses. When the 3-step procedure for finding traumatic CMBs from FA maps was implemented separately for the *first* timepoint, only 14 CMBs (8%) were found to be of likely traumatic etiology ($q < 0.05$). When the procedure was implemented for the *second* timepoint, only 5 such CMBs (3%) were found, and the 2 sets of CMBs did not overlap. However, all 19 CMBs (11%) were among those already evaluated as being of likely traumatic etiology based on the analysis of longitudinal data.

When using MD, RD, or AD maps, the numbers of mTBI participants identified as CMB$^+$ were 54, 44, and 60, respectively. The number of CMBs likely to be traumatic was found to be 78 (45%, MD), 65 (38%, RD) and 112 (65%, AD). Cross-sectionally, the use of MD alone led to the identification of 4 traumatic CMBs (2%) at the first timepoint and of 6 such CMBs (3%) at the second timepoint. For RD, the numbers of traumatic CMBs were 2 (1%) and 5 (3%), respectively. For AD, they were 11 CMBs (6%) and 21 CMBs (12%), respectively. Since MD, RD and AD were not as useful as FA to identify CMBs, we chose FA as the diffusion metric of choice for the remainder of the analysis but retained the other measures to interrogate associations with cognitive function change.

3.2. WM changes with distance from CMBs

The null hypothesis that a CMB's mean *proximal* FA change was equal to its mean *distal* FA change was rejected for 144 (87%) CMBs across 57 (92%) participants (all $q < 0.05$). This null hypothesis was rejected for 2.6 ± 2.3 CMBs per participant (range: 1–7; median: 2). Across participants, mean FAs decreased by 34% ± 11% (range: 6%-59%) in regions proximal to CMBs and by 11% ± 9% (range: 0%–26%) in those distal to CMBs. Proximal FA decreases were significantly correlated with age at injury (r = 0.45, t_{60} = 3.90, $p = 1.2 \times 10^{-4}$); male sex was associated with significantly larger FA decreases (r = 0.34, t_{60} = 2.80, p = 0.003). The age-by-sex interaction was found to modulate proximal FA decreases significantly ($F_{9,\ 14} = 3.02$, p = 0.03). Representative examples of CMBs relative to the cerebrum and to their nearest WM fasciculi are displayed in Fig. 5. When the null hypothesis was tested separately for each timepoint, it was rejected for only 12 CMBs (7%) across 5 (8%) participants (all $q < 0.05$) at the acute baseline timepoint. At the chronic follow-up timepoint, the hypothesis was rejected for only 8 CMBs (5%) across 7 (11%) participants (all $q <$ 0.05).

3.3. WM changes along individual streamlines with distance from CMBs

Across mTBI volunteers, 97.1% ± 2.1% ($\mu \pm \sigma$) WM tracts (streamlines) harboring CMBs exhibited lowest FAs closest to the CMB, with FA increasing to normal (expected) values as the distance from the CMB increased (Fig. 3). FA decreases became significantly smaller as the topological distance to the CMB increased (all $q < 0.05$). In other words, in the average mTBI participant, ~97% of WM structures harboring CMBs exhibited FA decreases along prototype streamlines. The magnitude of such decreases was significantly and negatively correlated with the along-streamline distance to the nearest CMBs (Fig. 3). The correlation coefficient between FA decreases and CMB distances averaged 0.63 ± 0.21 across participants. This correlation is significantly different from zero (t_{61} = 6.28, $p = 2.05 \times 10^{-8}$). When the correlation coefficient between FA (rather than FA *changes*) and CMB distances was computed separately for the first timepoint, it was found to average only 0.02 ± 0.06 across participants, a statistically insignificant correlation (t_{61} = 0.11, p = 0.44). For the second timepoint, the correlation averaged 0.07 ± 0.08 (t_{61} = 0.21, p = 0.43).

3.4. Relation between WM changes near CMBs versus cognitive decline

Significant correlations ($q < 0.05$) were found between changes in cognitive functions quantified by MoCA, on the one hand, and WM structures' mean FA, MD, and RD changes near CMBs, on the other hand (Table 2). Each participant exhibited change(s) in the MoCA subscore(s) for *at least one* cognitive domain. MoCA subscore changes pertained to attention (N = 36 or 58% of the sample), executive functions (N = 41 or 66%), memory (N = 39 or 63%), language (N = 33 or 53%), visuo-constructional ability (N = 37 or 60%), and orientation (N = 31 or 50%). Decreases in MoCA subscores for some cognitive domains were compensated by increases in others, resulting in the mean MoCA score of the mTBI sample increasing from 27 at acute baseline to 28 at chronic follow-up. All participants with CMBs were included in each statistical test of the relation between cognitive changes and WM changes near CMBs. Callosal CMBs exhibiting FA changes proximal to CMBs were associated with change in MoCA sub-scores across all cognitive domains: attention, executive control, memory, language, and visuo-constructional abilities (Fig. 6, Fig. 7, all $q < 0.05$). Similarly, CMB-related FA changes in the cingulum bundle were statistically associated with all sub-scores, excepting language (Fig. 6, Fig. 7, all $q < 0.05$). Other WM fasciculi exhibiting CMB-related FA decreases associated with cognitive decline included the inferior longitudinal fasciculus (executive functions, language, etc.), inferior occipito-frontal and middle longitudinal fasciculi (attention, language, etc.), and the corona radiata (executive functions, orientation), as illustrated in Fig. 6 and Fig. 7. Significant CMB-related changes in MD and RD were found primarily in the corpus callosum, but other structures also featured CMB-related changes in either or both measures, except for the corona radiata (Table 2).

Cross-sectionally, correlations were computed at each timepoint between cognitive functions quantified by MoCA scores (rather than by MoCA score *changes*), and WM structures' mean FA (rather than FA *changes*) near CMBs. The only statistically significant associations were between (A) baseline attention and the mean FA of the corpus callosum (r = 0.42, t_{23} = 2.22, q = 0.05), and between (2) baseline visuo-constructional ability and the mean FA of the inferior longitudinal fasciculus (r = 0.36, t_{18} = 1.85, q = 0.05).

4. Discussion

After moderate-to-severe TBI, it is common to find intraparenchymal hemorrhages, mass effect and edema on clinical MRIs. Often, this contributes to TBI heterogeneity and complicate group-level neuroimage analysis. Our study focuses on mTBI, which includes participants whose only radiological findings were CMB-related susceptibility changes on SWI. Thus, our study benefits from the considerable advantage of examining CMB correlates in the absence of gross pathology on MRI, which might otherwise confound our findings. In this study, CMB$^+$ HCs are significantly older than mTBI participants. Obtaining data from younger

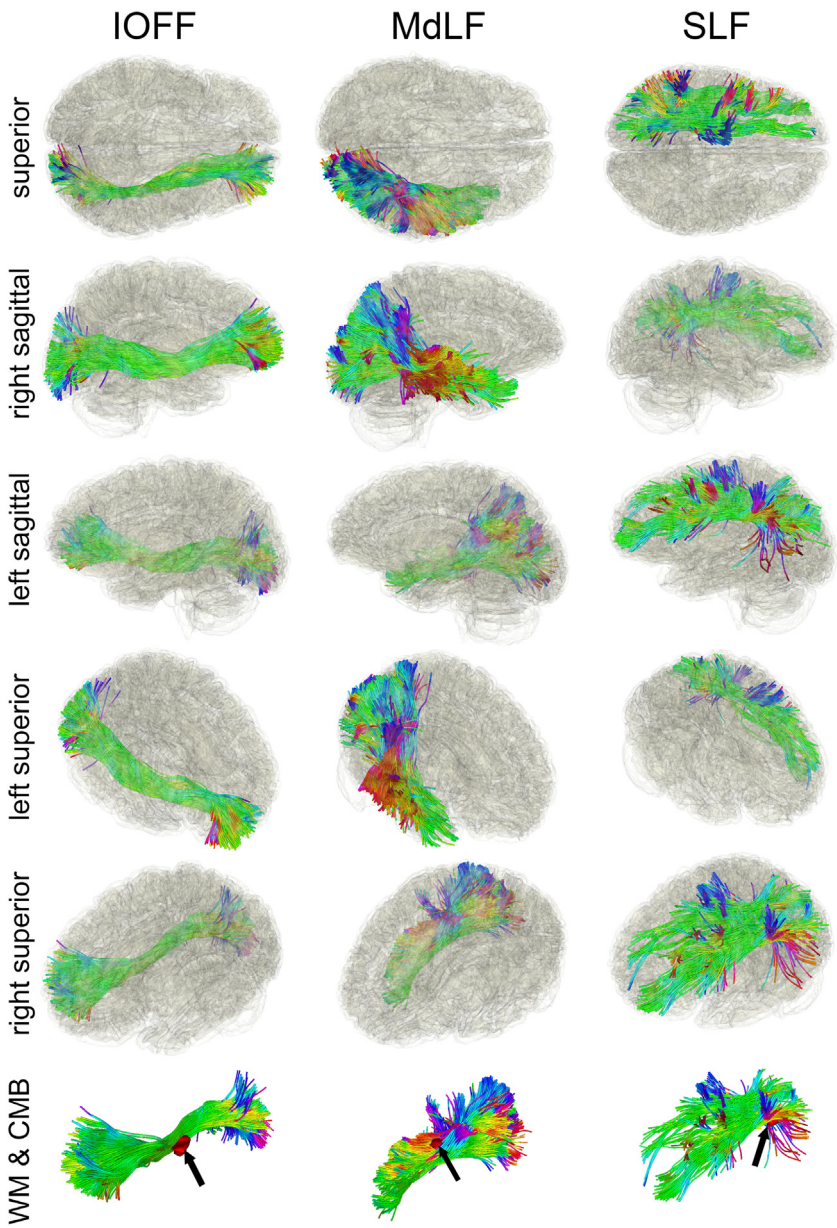

Fig. 5. CMBs relative to major WM structures. Examples of CMBs (red objects pointed to by black arrows) are displayed relative to the cerebrum and to their nearest WM fasciculi (first column: IOFF; second column: MdLF; third column: SLF). WM streamline colors encode fiber orientation (red: left – right; green: anterior – posterior; blue: inferior – superior). Each row depicts the brain from a different viewpoint. The gray matter surface is translucent in all rows except that at the bottom of the figure, where only the WM streamlines and the CMBs are shown. (For interpretation of the references to color in this figure legend, the reader is referred to the Web version of this article.)

CMB^+ HCs is difficult partly due to the relatively low incidence of CMBs in young and middle-aged adults without neurological disease (Poels et al., 2010). Nevertheless, the significantly older mean age of CMB^+ HCs can be perceived as a strength because WM integrity decreases with age overall (Kochunov et al., 2011), such that older CMB^+ HCs presumably have lower FAs than younger CMB^+ HCs (Grieve et al., 2007). Thus, a HC group significantly older than the mTBI study group could provide useful insight in a study like ours because the average WM integrity difference between mTBI participants and older HCs is presumably greater than between the former and younger HCs.

A tractography-based approach like ours is necessary for the calculation of topological distances along WM streamlines. Whereas region-of-interest approaches allow one to map WM changes within such regions, these methods do not facilitate the calculation of along-streamline distances from a CMB. Since fluid diffusion within WM is anisotropic, it is prudent to assume that the spread of blood compounds away from a CMB is also anisotropic. Thus, a tractography framework was deemed to be appropriate for capturing the anisotropic effects of CMBs upon WM streamlines as a function of *topological* (i.e., along-streamline, rather than *Euclidean*) distance to the nearest CMB.

Our choice of FA over other diffusion metrics (MD, RD, AD) is partly justified by our poor ability to identify CMBs of likely traumatic etiology using any of these latter 3 metrics. Importantly, the ability of each diffusion metric to identify traumatic CMBs relies on statistical effect sizes that also constrain the power of our ulterior

Table 2
Differential vulnerability of major WM structures to CMB-related cognitive change

Structure	*N*	*Cognitive ability*	*Measure*	*r*	*t*	*q*
corpus callosum	25	attention	FA	0.52	2.92	0.01
			MD	0.44	2.35	0.02
			RD	0.45	2.42	0.01
		executive functions	FA	0.39	2.03	0.03
			MD	0.37	1.91	0.03
			RD	0.61	3.69	0.01
		memory	FA	0.52	2.92	0.01
			MD	0.50	2.77	0.01
		language	FA	0.42	2.22	0.02
			RD	0.35	1.79	0.01
		visuo-constructional	FA	0.41	2.22	0.01
			MD	0.39	2.03	0.01
cingulum bundle	31	attention	FA	0.49	3.03	0.01
			RD	0.39	2.28	0.02
		executive functions	FA	0.42	2.49	0.01
			MD	0.48	2.95	0.01
		memory	FA	0.39	2.28	0.02
		visuo-constructional	FA	0.40	2.35	0.01
inferior longitudinal fasciculus	20	executive functions	FA	0.45	2.35	0.02
			MD	0.42	2.14	0.03
		memory	FA	0.41	2.13	0.04
		language	FA	0.37	1.96	0.05
		visuo-constructional	FA	0.40	1.91	0.04
inferior occipito-frontal fasciculus	39	attention	FA	0.39	2.58	0.01
			MD	0.35	2.27	0.02
			RD	0.38	2.50	0.01
		language	FA	0.37	2.42	0.01
		visuo-constructional	FA	0.51	3.61	0.03
middle longitudinal fasciculus	27	attention	FA	0.36	1.93	0.03
			RD	0.38	2.05	0.03
			MD	0.44	2.45	0.01
		language	FA	0.41	2.25	0.02
corona radiata	36	executive functions	MD	0.46	3.02	0.01
			FA	0.30	1.84	0.04
		orientation	MD	0.33	2.04	0.03
			FA	0.42	2.70	0.01

Listed are the results of testing the null hypothesis of no significant correlation r between (1) changes in MoCA sub-scores for individual cognitive abilities (second column) and (2) changes in diffusion properties near CMBs located within WM structures (first column). The null hypothesis was tested across all mTBI participants with CMBs at $\alpha = 0.05$ with multiple comparison corrections. The tabulation includes WM structure names, affected cognitive abilities quantified using MoCA, t statistics with degrees of freedom ($d.f.$) equal to N - 2, where N is the number of participants with CMBs in the respective structure, and FDR-corrected q values (second, fourth and fifth columns, respectively). Only statistically significant findings are listed.

statistical tests. Thus, unfortunately, the smaller effect sizes associated with MD, RD, and AD imply a paucity of findings based on these measures throughout the rest of the study and preclude our ability to gain comprehensive insights on post-traumatic pathology from MD, RD, or AD. In our context, the higher utility of FA compared to RD and AD may be due to the former metric being a function of all 3 DT eigenvalues, which could make it more sensitive to CMB-related WM changes. By contrast, RD is the average of 2 DT eigenvalues and AD is identically equal to the first eigenvalue of the DT. MD is the average of all 3 eigenvalues but may not be as useful as FA because the latter is a weighted sum of squared differences between each eigenvalue and the eigenvalue mean. Thus, FA is adjusted for eigenvalues' deviations from their mean, and this might render FA more sensitive to CMB-related changes in WM diffusion properties. The relative merit of various diffusion metrics in our context remains unclear, however, and future studies should investigate it further.

Our longitudinal analysis provides considerably broader findings linking CMBs to nearby changes in WM properties compared to the cross-sectional analysis. For example, based only on cross-sectional analysis of WM properties, only few CMBs of likely traumatic etiology could be identified. Similarly, cross-sectionally, WM near CMBs was found to differ significantly from distal WM only for a small minority of CMBs. Thirdly, the average correlation between the CMB-to-streamline distances and streamline FA was found to be insignificant, regardless of timepoint. Finally, the cross-sectional analysis identified only 2 significant associations between cognitive function and CMB-related WM properties, both at the acute baseline timepoint. These results suggest that the longitudinal component of our analysis can be critical for identifying significant CMB effects on WM, and that cross-sectional analysis may be insufficient. It is plausible that DTI-derived WM properties are insufficiently sensitive to CMB effects, such that these properties must be compared across timepoints to gain insight into WM degradation profiles.

Because our study establishes correlational (rather than causal) relationships linking CMBs, peri-hemorrhagic WM degradation, and cognitive deficits, our findings should be interpreted cautiously. WM changes between the time of injury and ~6 month follow-up can be interpreted in several ways: (1) although CMBs may be manifest at the time of mTBI, it takes time before myelin injured at the same time to degenerate (this scenario is consistent with differential delay in the manifest effects of mechanical injury), (2) breakdown in the blood-brain barrier at the time of mTBI as reflected by CMBs may lead to progressive WM degeneration over time (this scenario is consistent with progressive neurotoxic effects on WM triggered by breakdown in the BBB). Finally, since CMB findings on MRI are non-specific and may result from vascular or traumatic etiologies, it is conceivable that TBI effects on pre-traumatic CMBs could lead to WM change near CMBs despite

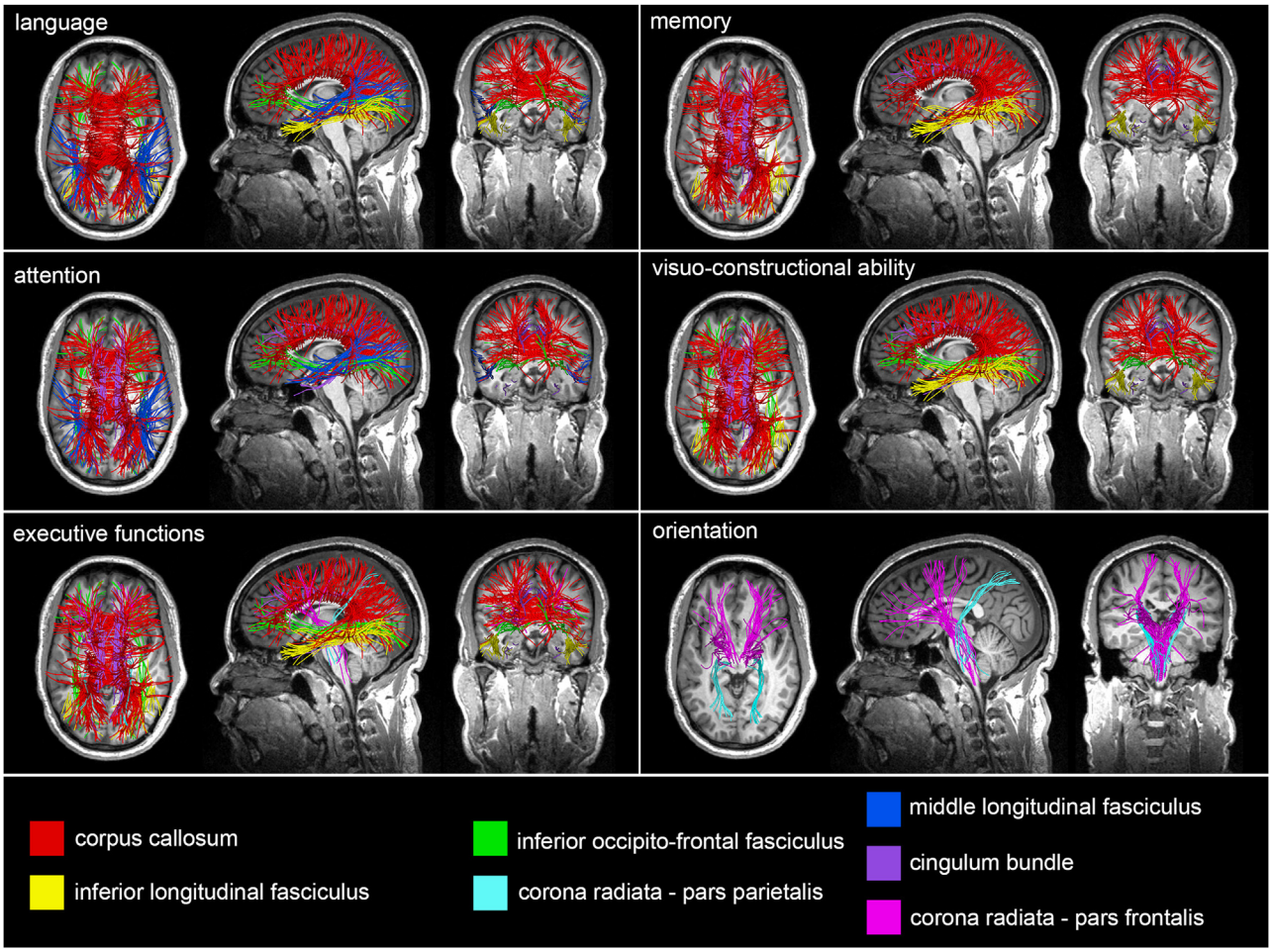

Fig. 6. WM changes involving CMB-related cognitive changes. Significant changes in WM structure (all $q < 0.05$) involve language, attention, executive functions, memory, orientation, and visuo-constructional ability. Each WM structure displayed exhibits CMB-related diffusion property changes that are significantly associated with cognitive change in the respective cognitive ability. Callosal CMBs exhibiting WM changes near CMBs are associated with changes in attention, executive control, memory, language, and visuo-constructional abilities. CMB-related FA changes in the cingulum bundle are statistically associated with changes across all sub-scores, excepting language. Other WM fasciculi with CMB-related FA decreases included the inferior longitudinal fasciculus (executive functions, language, etc.), inferior occipito-frontal and middle longitudinal fasciculi (attention, language, etc.), and the corona radiata (executive functions, orientation, etc.).

these being pre-traumatic. For example, preexisting hypertension and CAA (Irimia et al., 2018; Iscan et al., 2015) are relatively frequent in older mTBI patients (Thompson et al., 2012), and these conditions can lead to CMBs. It is possible that TBI could, through mechanisms unknown to us, affect pre-traumatic CMBs in ways that result in WM changes similar to those that we associate here with traumatic CMBs. Should this be the case, the correlations of pre-traumatic CMBs with lower FAs relative to normotensive patients (Burgmans et al., 2010) may affect our findings in ways that we cannot assess.

Here we introduce a procedure to estimate the probability of each CMB's pathogenesis being related to trauma. In participants with mTBI, we compared mean FA changes in the vicinity of CMBs to the mean FA changes observed near these CMBs in persons without mTBI (HCs) across comparable time intervals. The results of this comparison suggested that mTBI participants' mean FA decreases were significantly larger than those of CMB^+ HCs. Due to the relatively slow rate of CAA progression compared to the time scale of acute mTBI dynamics; this weakens the case for the scenario in which CAA is causal to most CMBs studied here. Nevertheless, the possibility that some of our findings are due to preexisting neurovascular disease and/or to other non-traumatic biological processes must be acknowledged.

Our study shows that (1) traumatic CMBs are associated with greatest FA decreases within a ~10 mm radius from CMBs and that (2) these FA decreases drop off in magnitude with increasing distance from the CMBs. Because FA decreases typically reflect WM degradation (Inglese et al., 2005), these findings parallel those of experiments describing CMB-related parenchymal releases of neurotoxic compounds, which then infiltrate along axons to affect WM bundles near CMBs (Kenney et al., 2016). However, our observed FA changes could also result from mechanical stress gradients that affect both blood vessels and surrounding WM.

Male sex and older age were found here to be associated with larger FA decreases relative to females and younger patients, respectively. Thus, these demographic descriptors may increase the risk for CMB-related WM degradation. In this context, our findings help to reveal how mTBI-related neurodegeneration is modulated by sex and age at injury, an understudied research topic (Thompson et al., 2006). Nevertheless, because our follow-up period covers only the first ~6 months post-injury, our inferences may not reflect the entire trajectory of mTBI evolution, which future studies should evaluate.

Our results suggest that the associations between CMB effects on WM and cognitive deficits are modulated by relationships linking CMBs to degradation within individual WM tracts. CMB^+ WM

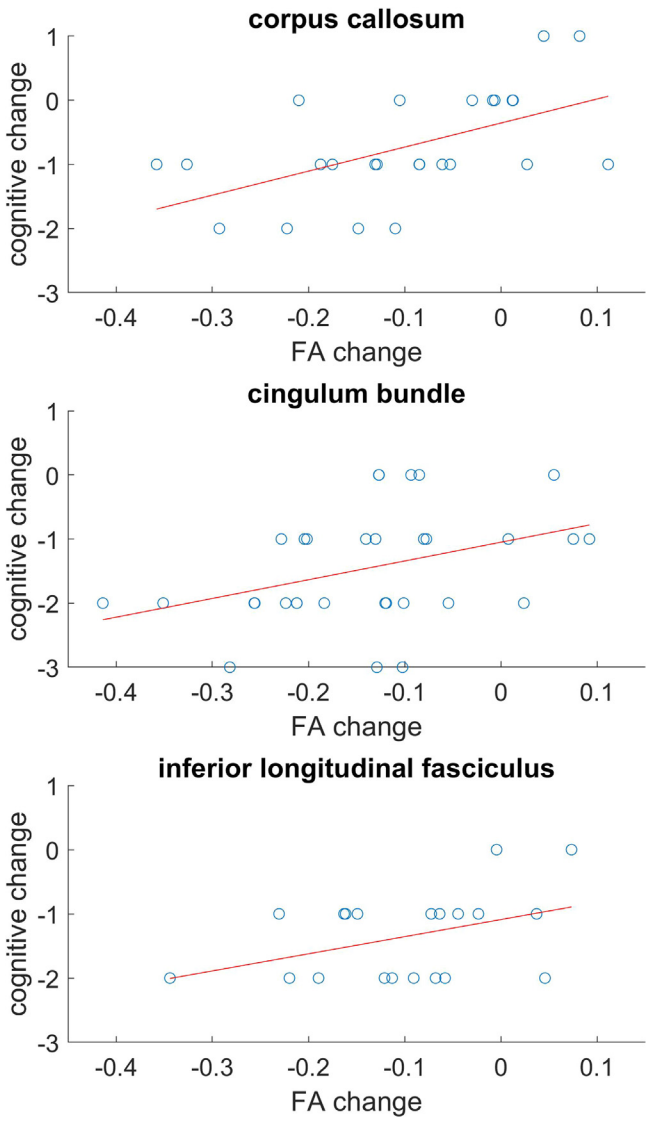

Fig. 7. MoCA memory subscore changes as a function of mean FA change. Significant mean FA changes (horizontal axis) within 3 representative structures (corpus callosum, cingulum bundle, and inferior longitudinal fasciculus) are paralleled by MoCA memory subscore changes (vertical axis). Each circle denotes a participant; the line of best linear fit is displayed in red (see also Table 2). (For interpretation of the references to color in this figure legend, the reader is referred to the Web version of this article.)

structures most strongly associated with such deficits are the corpus callosum, cingulum bundle, the inferior fronto-occipital fasciculus, inferior/middle longitudinal fasciculus, and the corona radiata. This is consistent with biomechanical models indicating that the stretching, twisting, and/or shearing of axons in these large WM structures can collectively reflect the typical range and directions of brain movement during coup-contrecoup occurrences of traumatic acceleration/deceleration (Ji et al., 2014). Of note, however, our analysis may have failed to identify significant associations between cognitive decline and the FA of certain small WM tracts simply because, in principle, small tracts are less likely to be affected by CMBs unless they are in WM regions particularly prone to CMBs. Future studies in larger samples should seek to identify such small tracts.

The WM structures listed in Table 2 modulate a preponderance of cognitive functions affected detrimentally by mTBI. For example, the corpus callosum and cingulum bundles modulate attention, executive control, and other functions requiring interhemispheric information exchange (Bubb et al., 2018; Quigley et al., 2003). Similarly, the occipito-frontal and middle longitudinal fasciculi have well-documented roles in language (Turken and Dronkers, 2011). Thus, our findings are consistent with the hypothesis that CMB-related WM degradation is associated with deficits in cognitive functions mediated by fasciculi containing CMBs. Somewhat unexpectedly, however, CMB counts were not associated significantly with acute GCS score, LOC duration, PTA duration or chronic MoCA scores. Because we focused on mTBI, there was less variability in GCS and duration of LOC (less than 30 minutes by definition) than in moderate-to-severe mTBI. Alternatively, CMB count may not reflect the focal, WM changes surrounding CMB that drive post-traumatic changes in these neurocognitive measures. This subtlety of effects may also indicate why CMBs have often been perceived as clinically silent, and why methodological approaches like ours might be necessary further to study the clinical significance of CMB findings. A limitation of our study is that, for logistical reasons, MRIs were typically acquired several days after MoCA. However, it is unknown how soon cognition should be evaluated after injury to optimize correlations with neuroimaging measures (Calvillo and Irimia, 2020). Because cognitive scores acquired sooner post-injury may better reflect neuroanatomic trajectories (Irimia et al., 2012), future studies should investigate this.

Previous studies correlating CMBs with surrounding WM changes have been challenging because there are few reliable methods for DTI longitudinal analysis of WM connections. Furthermore, because few longitudinal DTI methods have been leveraged to study CMB associations with WM changes, our results cannot be compared directly with those of previous studies. Tract-based spatial statistics (TBSS) offers a standard strategy for within- and between-participant comparison of DTI volumes (Smith et al., 2006). Although useful for voxel-wise analysis of WM properties, TBSS does not accommodate calculations of FA changes along WM fibers. By contrast, our approach uses a detailed WM atlas to delineate WM bundles reproducibly and to cluster them (O'Donnell and Westin, 2007). When integrated with streamline prototyping and with Riemannian streamline matching like in our study, TBM facilitates the identification of WM connectivity and its changes (Calvillo and Irimia, 2020; O'Donnell and Westin, 2007; O'Donnell et al., 2009; Rostowsky et al., 2018). Although methods like differential tractography (Yeh et al., 2019) are promising, these approaches have not been validated for studies like ours.

Our findings suggest that CMBs affect nearby WM considerably more than distant WM. Thus, CMBs close to one another may interact statistically and mechanistically in how they mediate WM changes. Statistical interactions between multiple CMBs and their aggregate effects upon WM were not considered because our analysis examined only the correlative relationship between spatially isolated CMBs and the properties of surrounding WM. However, because CMBs may occur in spatial clusters (Mesker et al., 2011), future studies should investigate statistical effects pertaining to interactions between CMBs.

5. Conclusion

This study leveraged atlas-informed WM labeling, DTI streamline prototyping and Riemannian streamline matching to quantify CMB-related WM degradation after mTBI. Of note, we presented evidence suggesting that CMBs of likely traumatic etiology can be associated with substantial degradation of surrounding WM. Our findings indicate that such degradation can be associated with decline in cognitive functions mediated by WM fasciculi containing CMBs. Thus, our study challenges the hypothesis that traumatic

CMBs are clinically silent. Instead, our findings underline the vulnerability to cognitive deficits that may characterize CMB^{+} mTBI victims. Because such patients may be at relatively higher risk for WM damage and cognitive decline, they may benefit from personalized clinical evaluation and outcome prognostication based on their age at injury and sex, above and beyond what is warranted for CMB^{-} mTBI patients with otherwise similar clinical profiles.

Ethics approval

This study was conducted with the approval of the Institutional Review Board at the University of Southern California and was carried out in accordance with the Declaration of Helsinki and with the U.S. Code of Federal Regulations (45 C.F.R. 46).

Consent to participate

All participants provided written informed consent.

Consent for publication

All authors approved the final version of the manuscript for publication.

Availability of data and material

Primary data generated and/or analyzed during this study can be made available subject to a data transfer agreement. At the request of some participants, their written permission is additionally required in some cases.

Code availability

FreeSurfer (https://surfer.nmr.mgh.harvard.edu), the FMRIB Software Library (https://fsl.fmrib.ox.ac.uk) and the Slicer dMRI white matter clustering software (https://github.com/SlicerDMRI/whitematteranalysis) are freely available. Other software used in this study is available from the corresponding author upon request, subject to an intellectual property agreement.

Authors' contributions

Authors contributed to study design (A.I., S.H.J., F.Z., L.J.O., N.S.B., X.Z., H.C.C.), data analysis (A.I., V.N., K.A.R., N.N.C., A.D., F.Z., S.H.J.), result interpretation (A.I., V.N., K.A.R., N.N.C., A.D., A.N.P., F.Z., S.H.J., L.J.O., N.S.B., X.Z., H.C.C.), and to manuscript redaction (A.I., A.N.P, N.S.B., X.Z., H.C.C.).

Disclosure statement

The authors declare that this research was conducted with no commercial or financial relationships that could be construed as a potential conflict of interest statement.

Acknowledgements

This work was supported by NIH grant R01 NS 100973 to A.I., by DoD award W81-XWH-1810413 to A.I., by a James and Sue Femino Foundation grant to A.I., by a Hanson-Thorell Research Scholarship to A.I., and by funding from both the Undergraduate Research Associate Program (URAP) and the Center for Undergraduate Research in Viterbi Engineering (CURVE) at the University of Southern California. L.J.O. and F.Z. were supported by NIH grants R01 MH 119222, R01 MH 125860, P41 EB 015902, and R01 MH 074794. The funders had no role in the preparation of this article.

The authors are grateful to Ammar Dharani, Nahian F. Chowdhury, Jun H. Kim, Hyung-Jun Lee, Dylan Overby, David J. Robles, Kenneth A. Rostowsky, Chur M. Tam and Shania H. Wang for their assistance.

References

Andersson, J.L., Skare, S., Ashburner, J., 2003. How to correct susceptibility distortions in spin-echo echo-planar images: application to diffusion tensor imaging. Neuroimage 20 (2), 870–888. doi:10.1016/S1053-8119(03)00336-7.

Bigler, E.D., Maxwell, W.L., 2012. Neuropathology of mild traumatic brain injury: relationship to neuroimaging findings. Brain Imaging Behav 6 (2), 108–136. doi:10.1007/s11682-011-9145-0.

Bubb, E.J., Metzler-Baddeley, C., Aggleton, J.P., 2018. The cingulum bundle: anatomy, function, and dysfunction. Neurosci Biobehav Rev 92, 104–127. doi:10.1016/j.neubiorev.2018.05.008.

Burgmans, S., van Boxtel, M.P., Gronenschild, E.H., Vuurman, E.F., Hofman, P., Uylings, H.B., Jolles, J., Raz, N., 2010. Multiple indicators of age-related differences in cerebral white matter and the modifying effects of hypertension. Neuroimage 49 (3), 2083–2093. doi:10.1016/j.neuroimage.2009.10.035.

Calvillo, M., Irimia, A., 2020. Neuroimaging and psychometric assessment of mild cognitive impairment after traumatic brain injury. Front Psychol 11, 1423. doi:10.3389/fpsyg.2020.01423, article.

Eierud, C., Craddock, R.C., Fletcher, S., Aulakh, M., King-Casas, B., Kuehl, D., LaConte, S.M., 2014. Neuroimaging after mild traumatic brain injury: review and meta-analysis. Neuroimage Clin 4, 283–294. doi:10.1016/j.nicl.2013.12.009.

Glushakova, O.Y., Johnson, D., Hayes, R.L., 2014. Delayed increases in microvascular pathology after experimental traumatic brain injury are associated with prolonged inflammation, blood-brain barrier disruption, and progressive white matter damage. J Neurotrauma 31 (13), 1180–1193. doi:10.1089/neu.2013.3080.

Grieve, S.M., Williams, L.M., Paul, R.H., Clark, C.R., Gordon, E., 2007. Cognitive aging, executive function, and fractional anisotropy: a diffusion tensor MR imaging study. AJNR Am J Neuroradiol 28 (2), 226–235.

Hellyer, P.J., Leech, R., Ham, T.E., Bonnelle, V., Sharp, D.J., 2013. Individual prediction of white matter injury following traumatic brain injury. Ann Neurol 73 (4), 489–499. doi:10.1002/ana.23824.

Inglese, M., Makani, S., Johnson, G., Cohen, B.A., Silver, J.A., Gonen, O., Grossman, R.I., 2005. Diffuse axonal injury in mild traumatic brain injury: a diffusion tensor imaging study. J Neurosurg 103 (2), 298–303. doi:10.3171/jns.2005.103.2.0298.

Irimia, A., Chambers, M.C., Torgerson, C.M., Filippou, M., Hovda, D.A., Alger, J.R., Gerig, G., Toga, A.W., Vespa, P.M., Kikinis, R., Van Horn, J.D., 2012. Patient-tailored connectomics visualization for the assessment of white matter atrophy in traumatic brain injury. Front Neurol 3, 10. doi:10.3389/fneur.2012.00010.

Irimia, A., Torgerson, C.M., Goh, S.Y., Van Horn, J.D., 2015. Statistical estimation of physiological brain age as a descriptor of senescence rate during adulthood. Brain Imaging Behav 9 (4), 678–689. doi:10.1007/s11682-014-9321-0.

Irimia, A., Van Horn, J.D., Vespa, P.M., 2018. Cerebral microhemorrhages due to traumatic brain injury and their effects on the aging human brain. Neurobiol Aging 66, 158–164. doi:10.1016/j.neurobiolaging.2018.02.026.

Iscan, Z., Jin, T.B., Kendrick, A., Szeglin, B., Lu, H., Trivedi, M., Fava, M., McGrath, P.J., Weissman, M., Kurian, B.T., Adams, P., Weyandt, S., Toups, M., Carmody, T., McInnis, M., Cusin, C., Cooper, C., Oquendo, M.A., Parsey, R.V., DeLorenzo, C., 2015. Test-retest reliability of freesurfer measurements within and between sites: effects of visual approval process. Hum Brain Mapp 36 (9), 3472–3485. doi:10.1002/hbm.22856.

Jeerakathil, T., Wolf, P.A., Beiser, A., Hald, J.K., Au, R., Kase, C.S., Massaro, J.M., DeCarli, C., 2004. Cerebral microbleeds: prevalence and associations with cardiovascular risk factors in the Framingham Study. Stroke 35 (8), 1831–1835. doi:10.1161/01.STR.0000131809.35202.1b.

Ji, S., Ghadyani, H., Bolander, R.P., Beckwith, J.G., Ford, J.C., McAllister, T.W., Flashman, L.A., Paulsen, K.D., Ernstrom, K., Jain, S., Raman, R., Zhang, L., Greenwald, R.M., 2014. Parametric comparisons of intracranial mechanical responses from three validated finite element models of the human head. Ann Biomed Eng 42 (1), 11–24. doi:10.1007/s10439-013-0907-2.

Joshi, S.H., Klassen, E., Srivastava, A., Jermyn, I., 2007. A novel representation for Riemannian analysis of elastic curves in R-n. Proc Cvpr Ieee 1643-+. doi:10.1109/CVPR.2007.383185.

Kenney, K., Amyot, F., Haber, M., Pronger, A., Bogoslovsky, T., Moore, C., Diaz-Arrastia, R., 2016. Cerebral vascular injury in traumatic brain injury. Exp Neurol 275 (Pt 3), 353–366. doi:10.1016/j.expneurol.2015.05.019.

Kochunov, P., Glahn, D.C., Lancaster, J., Thompson, P.M., Kochunov, V., Rogers, B., Fox, P., Blangero, J., Williamson, D.E., 2011. Fractional anisotropy of cerebral white matter and thickness of cortical gray matter across the lifespan. Neuroimage 58 (1), 41–49. doi:10.1016/j.neuroimage.2011.05.050.

Liao, R., Ning, L., Chen, Z., Rigolo, L., Gong, S., Pasternak, O., Golby, A.J., Rathi, Y., O'Donnell, L.J., 2017. Performance of unscented Kalman filter tractography in edema: Analysis of the two-tensor model. Neuroimage Clin 15, 819–831. doi:10.1016/j.nicl.2017.06.027.

Lok, J., Leung, W., Murphy, S., Butler, W., Noviski, N., Lo, E.H., 2011. Intracranial hemorrhage: mechanisms of secondary brain injury. Acta Neurochir Suppl 111, 63–69. doi:10.1007/978-3-7091-0693-8_11.

Martinez-Ramirez, S., Greenberg, S.M., Viswanathan, A., 2014. Cerebral microbleeds: overview and implications in cognitive impairment. Alzheimers Res Ther 6 (3), 33. doi:10.1186/alzrt263.

Mesker, D.J., Poels, M.M., Ikram, M.A., Vernooij, M.W., Hofman, A., Vrooman, H.A., van der Lugt, A., Breteler, M.M., 2011. Lobar distribution of cerebral microbleeds: the Rotterdam Scan Study. Arch Neurol 68 (5), 656–659. doi:10.1001/archneurol.2011.93.

Mosenthal, A.C., Livingston, D.H., Lavery, R.F., Knudson, M.M., Lee, S., Morabito, D., Manley, G.T., Nathens, A., Jurkovich, G., Hoyt, D.B., Coimbra, R., 2004. The effect of age on functional outcome in mild traumatic brain injury: 6-month report of a prospective multicenter trial. J Trauma 56 (5), 1042–1048. doi:10.1097/01.ta.0000127767.83267.33.

Nasreddine, Z.S., Phillips, N.A., Bedirian, V., Charbonneau, S., Whitehead, V., Collin, I., Cummings, J.L., Chertkow, H., 2005. The Montreal Cognitive Assessment, MoCA: a brief screening tool for mild cognitive impairment. J Am Geriatr Soc 53 (4), 695–699. doi:10.1111/j.1532-5415.2005.53221.x.

O'Donnell, L.J., Westin, C.F., 2007. Automatic tractography segmentation using a high-dimensional white matter atlas. IEEE T Med Imaging 26 (11), 1562–1575. doi:10.1109/Tmi.2007.906785.

O'Donnell, L.J., Westin, C.F., Golby, A.J., 2009. Tract-based morphometry for white matter group analysis. Neuroimage 45 (3), 832–844. doi:10.1016/j.neuroimage.2008.12.023.

Park, J.H., Park, S.W., Kang, S.H., Nam, T.K., Min, B.K., Hwang, S.N., 2009. Detection of traumatic cerebral microbleeds by susceptibility-weighted image of MRI. J Korean Neurosurg Soc 46 (4), 365–369. doi:10.3340/jkns.2009.46.4.365.

Petrault, M., Casolla, B., Ouk, T., Cordonnier, C., Berezowski, V., 2019. Cerebral microbleeds: Beyond the macroscope. Int J Stroke 14 (5), 468–475. doi:10.1177/1747493019830594.

Poels, M.M., Vernooij, M.W., Ikram, M.A., Hofman, A., Krestin, G.P., van der Lugt, A., Breteler, M.M., 2010. Prevalence and risk factors of cerebral microbleeds: an update of the Rotterdam scan study. Stroke 41 (10 Suppl), S103–S106. doi:10.1161/STROKEAHA.110.595181.

Prasad, G., Joshi, S.H., Jahanshad, N., Villalon-Reina, J., Aganj, I., Lenglet, C., Sapiro, G., McMahon, K.L., de Zubicaray, G.I., Martin, N.G., Wright, M.J., Toga, A.W., Thompson, P.M., 2014. Automatic clustering and population analysis of white matter tracts using maximum density paths. Neuroimage 97, 284–295. doi:10.1016/j.neuroimage.2014.04.033.

Quigley, M., Cordes, D., Turski, P., Moritz, C., Haughton, V., Seth, R., Meyerand, M.E., 2003. Role of the corpus callosum in functional connectivity. AJNR Am J Neuroradiol 24 (2), 208–212.

Robles, D.J., Dharani, A., Rostowsky, K.A., Chaudhari, N.N., Ngo, V., Zhang, F., O'Donnell, L.J., Green, L., Sheikh-Bahaei, N., Chui, H.C., Irimia, A., 2022. Older age, male sex, and cerebral microbleeds predict white matter loss after traumatic brain injury. Geroscience 44 (1), 83–102. doi:10.1007/s11357-021-00459-2.

Rostowsky, K.A., Maher, A.S., Irimia, A., 2018. Macroscale white matter alterations due to traumatic cerebral microhemorrhages are revealed by diffusion tensor imaging. Front Neurol 9. doi:10.3389/fneur.2018.00948.

Sehgal, V., Delproposto, Z., Haacke, E.M., Tong, K.A., Wycliffe, N., Kido, D.K., Xu, Y., Neelavalli, J., Haddar, D., Reichenbach, J.R., 2005. Clinical applications of neuroimaging with susceptibility-weighted imaging. J Magn Reson Imaging 22 (4), 439–450. doi:10.1002/jmri.20404.

Shenton, M.E., Hamoda, H.M., Schneiderman, J.S., Bouix, S., Pasternak, O., Rathi, Y., Vu, M.A., Purohit, M.P., Helmer, K., Koerte, I., Lin, A.P., Westin, C.F., Kikinis, R., Kubicki, M., Stern, R.A., Zafonte, R., 2012. A review of magnetic resonance imaging and diffusion tensor imaging findings in mild traumatic brain injury. Brain Imaging Behav 6 (2), 137–192. doi:10.1007/s11682-012-9156-5.

Smith, S.M., Jenkinson, M., Johansen-Berg, H., Rueckert, D., Nichols, T.E., Mackay, C.E., Watkins, K.E., Ciccarelli, O., Cader, M.Z., Matthews, P.M., Behrens, T.E.J., 2006. Tract-based spatial statistics: voxelwise analysis of multi-subject diffusion data. Neuroimage 31 (4), 1487–1505. doi:10.1016/j.neuroimage.2006.02.024.

Srivastava, A., Klassen, E., Joshi, S.H., Jermyn, I.H., 2011. Shape analysis of elastic curves in Euclidean Spaces. Ieee T Pattern Anal 33 (7), 1415–1428. doi:10.1109/Tpami.2010.184.

Tate, D.F., Gusman, M., Kini, J., Reid, M., Velez, C.S., Drennon, A.M., Cooper, D.B., Kennedy, J.E., Bowles, A.O., Bigler, E.D., Lewis, J.D., Ritter, J., York, G.E., 2017. Susceptibility weighted imaging and white matter abnormality findings in service members with persistent cognitive symptoms following mild traumatic brain injury. Mil Med 182 (3), e1651–e1658. doi:10.7205/MILMED-D-16-00132.

Thompson, H.J., Dikmen, S., Temkin, N., 2012. Prevalence of comorbidity and its association with traumatic brain injury and outcomes in older adults. Res Gerontol Nurs 5 (1), 17–24. doi:10.3928/19404921-20111206-02.

Thompson, H.J., McCormick, W.C., Kagan, S.H., 2006. Traumatic brain injury in older adults: epidemiology, outcomes, and future implications. J Am Geriatr Soc 54 (10), 1590–1595. doi:10.1111/j.1532-5415.2006.00894.x.

Toth, A., Kovacs, N., Perlaki, G., Orsi, G., Aradi, M., Komaromy, H., Ezer, E., Bukovics, P., Farkas, O., Janszky, J., Doczi, T., Buki, A., Schwarcz, A., 2013. Multimodal magnetic resonance imaging in the acute and sub-acute phase of mild traumatic brain injury: can we see the difference? J Neurotrauma 30 (1), 2–10. doi:10.1089/neu.2012.2486.

Toth, L., Czigler, A., Horvath, P., Kornyei, B., Szarka, N., Schwarcz, A., Ungvari, Z., Buki, A., Toth, P., 2021. Traumatic brain injury-induced cerebral microbleeds in the elderly. Geroscience 43 (1), 125–136. doi:10.1007/s11357-020-00280-3.

Turken, A.U., Dronkers, N.F., 2011. The neural architecture of the language comprehension network: converging evidence from lesion and connectivity analyses. Front Syst Neurosci 5, 1. doi:10.3389/fnsys.2011.00001.

van der Eerden, A.W., van den Heuvel, T.L.A., Maas, M.C., Vart, P., Vos, P.E., Platel, B., Goraj, B.M., Manniesing, R., 2021. The radiological interpretation of possible microbleeds after moderate or severe traumatic brain injury: a longitudinal study. Neuroradiology doi:10.1007/s00234-021-02839-z.

Wu, X., Kirov, I.I., Gonen, O., Ge, Y., Grossman, R.I., Lui, Y.W., 2016. MR imaging applications in mild traumatic brain injury: an imaging update. J Radiology 279 (3), 693–707. doi:10.1148/radiol.16142535.

Yeh, F.C., Zaydan, I.M., Suski, V.R., Lacomis, D., Richardson, R.M., Maroon, J.C., Barrios-Martinez, J., 2019. Differential tractography as a track-based biomarker for neuronal injury. Neuroimage 202, 116131. doi:10.1016/j.neuroimage.2019.116131.

Zhang, F., Wu, Y., Norton, I., Rigolo, L., Rathi, Y., Makris, N., O'Donnell, L.J., 2018. An anatomically curated fiber clustering white matter atlas for consistent white matter tract parcellation across the lifespan. Neuroimage 179, 429–447. doi:10.1016/j.neuroimage.2018.06.027.